THE PHOENIX ATMOSPHERIC STRUCTURE EXPERIMENT (ASE): DATA PROCESSING AND SCIENTIFIC RESULTS

Paul Withers[1] **and D. C. Catling**[2]

[1]*Center for Space Physics, Boston University, 725 Commonwealth Avenue, Boston, MA 02215, USA (withers@bu.edu)*
[2]*Department of Earth and Space Sciences, University of Washington, Box 351310, Seattle, WA 98195-1310, USA*

ABSTRACT

The purpose of this report is to highlight certain aspects of the data processing and scientific results associated with the Atmospheric Structure Experiment (ASE) of the Phoenix Mars lander. This experiment presented some unique challenges because its hardware was essentially designed and built to fulfill engineering requirements before the Phoenix mission began, meaning that the involvement of atmospheric scientists in the performance of the experiment was extremely limited. Nonetheless, the reconstruction of the Phoenix trajectory and associated atmospheric structure was successfully accomplished.

Key words: Mars; Atmosphere; Phoenix; EDL.

1. INTRODUCTION

NASA's Mars Scout program selected the Phoenix mission for flight in 2003. Its science mission focused "on providing the ground truth for the 2002 Odyssey discovery of massive ice deposits hidden under surface soils in the circumpolar regions" (Smith et al. 2008). The objectives of this mission were: (1) to study the history of the ground-ice and its emplacement mechanisms, (2) to address the effect that subsurface ice has on the local surface geomorphology, (3) to characterize the climate and local weather of the landing site, and (4) to address the habitability of the icy soil (Smith et al. 2008; Arvidson et al. 2009; Smith et al. 2009). Much of the design of the Phoenix spacecraft, including those aspects relevant for cruise and entry, descent, and landing (EDL), derived from the mothballed "Mars Surveyor 2001 Lander" (Guinn et al. 2008; Desai et al. 2008; Grover et al. 2008). Phoenix launched on 4 August 2007 and successfully landed on Mars in the late afternoon (16.6 hrs) in the Vastitas Borealis or northern plains region on 25 May 2008 (Table 1). Data from its EDL have been used to obtain the first profile of atmospheric density, pressure, and temperature from the martian polar regions with a vertical range in excess of 100 km and vertical resolution of less than 1 km.

Table 1. Time and position of Phoenix landing.

Time[1] (UTC)	2008-05-25T23:38:24
Aerocentric latitude[2] (°N)	68.21878 ± 0.00006
Longitude[2] (°E)	234.24845 ± 0.000096
Radius[2] (km)	3376.2915 ± 0.0014
Elevation[3] (m)	-4131
L_s[4] (degrees)	76.6
Local true solar time[5] (hrs)	16.6

[1]Smith et al. (2009).
[2]Martin-Mur (personal communication, 28 May 2008). The landed latitude, longitude and radius, which are shown with 1σ uncertainties, were determined from Doppler tracking.
[3]Elevation is with respect to the areoid defined by the Mars Orbiter Laser Altimeter (MOLA) investigation, specifically 16 pixels per degree gridded MOLA data acquired from http://geo.pds.nasa.gov/missions/mgs/megdr.html (Smith et al. 2003).
[4]Calculated using http://www-mars.lmd.jussieu.fr/mars/time/martian_time.html.
[5]Calculated from tabulated time and position using SPICE tools provided by JPL's Navigation and Ancillary Information Facility (NAIF).

Table 2. Reconstructed conditions and their 1σ uncertainties at parachute deployment.

Altitude (km)	13.54	0.38
Areocentric latitude (°N)	68.265	0.030
Longitude (°E)	234.034	0.058
Atmosphere-relative speed (m s^{-1})	390.9	1.5
Angle of attack (deg)	4.90	0.71
Mach number	1.703	0.015

Table 3. Reconstructed conditions and their 1σ uncertainties at first ground contact.

Altitude (km)	1.10	1.49
Areocentric latitude (°N)	68.237	0.029
Longitude (°E)	234.311	0.054
Atmosphere-relative speed (m s^{-1})	6.1	3.6

The Experiment Data Records (EDRs, time series of velocity changes and angular velocities with 200 samples per second) from the Phoenix Atmospheric Structure Experiment are available from the NASA Planetary Data System at http://atmos.nmsu.edu/PDS/data/phxase_0001/ (Catling et al. 2008). The Reduced Data Records (RDRs, reconstructed trajectory and atmospheric structure) from the Phoenix Atmospheric Structure Experiment are also available from the NASA Planetary Data System, this time at http://atmos.nmsu.edu/PDS/data/phxase_0002/ (Withers et al. 2010). Production of the RDRs from the EDRs has been reported previously in Withers et al. (2010) and the first scientific results have been summarized previously in Withers & Catling (2010). Analyses of data from ASE for engineering purposes have also been undertaken (Desai et al. 2008; Blanchard 2009). The unique contribution of the current work is to bring those two themes together in a single package that is focused on the interests of readers with a strong interest in the technological challenges and scientific opportunities associated with entry, descent, landing and flight in planetary atmospheres.

Figure 1 shows the time series of smoothed axial accelerations recorded during entry. Unsmoothed axial accelerations only exceed their uncertainties below 65 km. Smoothing extends the vertical range of useful data up to 128 km. The entry interface, defined to occur at a radial distance of 3522.2 km, equivalent to an altitude of 145.9 km, occurred at $t = 1857.733$ seconds. All altitudes reported in this paper are radial distances above 3376.3 km, which is the radial distance to the landing site, not distances relative to an equipotential surface. Peak deceleration was 84 m s^{-2}. Parachute deployment is responsible for the sudden increase in the magnitude of the measured acceleration near $t = 2090$ seconds and lander separation is responsible for the increase in the variance of the measured acceleration near $t = 2160$ seconds. Other events that occurred during EDL can be identified by careful inspection of the acceleration measurements (Desai et al. 2008). The reconstructed atmosphere-relative speed is shown in Figure 2. Table 2 reports the reconstructed conditions at parachute deployment and Table 3 reports the reconstructed conditions at first ground contact. The speed at first ground contact was 6.1 ± 3.6 m s^{-1}, which compares favourably with the design value of "a few m s^{-1}" (Desai et al. 2008). This speed differs from zero by about 0.1% of the entry speed of 5600 m s^{-1} (speed in a Mars-centered inertial frame) and differs from the design value of "a few m s^{-1}" by even less, suggesting that the trajectory reconstruction process was extremely successful, including the reconstruction of Phoenix's attitude.

The remaining sections of this work focus first on data processing, then on scientific results. Section 2 demonstrates the importance of accurate knowledge of relevant reference frames. Section 3 demonstrates a novel method for reducing noise by averaging. Section 4 demonstrates an inconsistency between two independent determinations of the angle of attack history of Phoenix. Section 5 outlines a possible alternative method for determining atmospheric density that is based on angle of attack

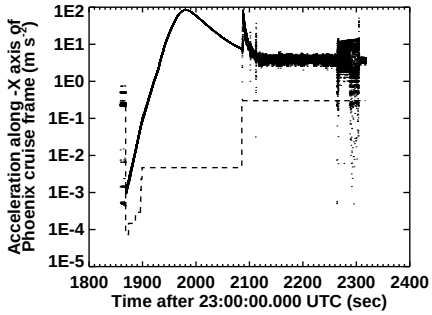

Figure 1. Smoothed axial accelerations (solid line) and 1σ uncertainties (dashed line). Uncertainties change as the width of the smoothing window decreases from 20 seconds at entry to 0.32 seconds during peak deceleration.

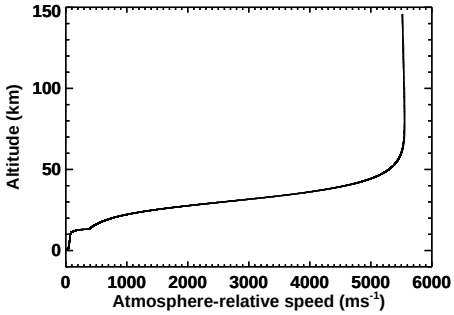

Figure 2. Atmosphere-relative speed as a function of altitude. In this frame, speed increases from 5517 m s^{-1} at entry to a maximum value of 5552 m s^{-1} at 81 km altitude. Acceleration due to gravity is more significant than deceleration due to aerodynamic drag in the rarefied upper atmosphere.

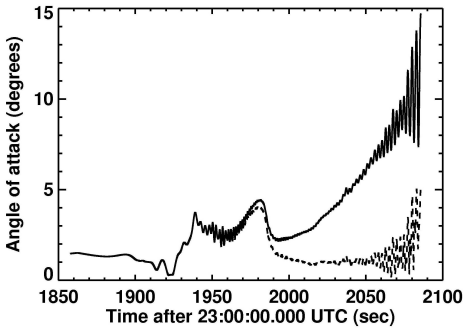

Figure 3. Reconstructed angle of attack using either the "as designed" matrix (solid line) or the "as built" matrix (dashed line). The choice of transformation matrix has dramatic implications for the reconstructed flight history.

oscillations. Section 6 outlines another possible alternative method for determining atmospheric density that uses Doppler-shifted radio transmissions during EDL. Section 7 presents and discusses the atmospheric results of the Phoenix Atmospheric Structure Experiment. Section 8 summarizes the findings of this work.

2. A GOOD SENSE OF DIRECTION

The time series of accelerations and angular velocities recorded during EDL that were originally archived as Experiment Data Records (EDRs) by the PDS (Catling et al. 2008) require a small correction (Withers et al. 2010). The raw data were transformed between several frames before being archived. One transformation matrix that was used in this process was based upon the spacecraft as designed, not as built. Elements of the "as built" matrix differ from the equivalent elements of the "as designed" matrix in the second or third decimal place. These apparently minor differences have major implications for the reconstructed trajectory and atmospheric structure. Altitude at parachute deployment varies by over 2 km depending on which version of this matrix is used, as does the altitude of first ground contact. The reconstructed angle of attack at parachute deployment, which can lead to mission failure if it is large, is a few degrees with the "as built" matrix, but over ten degrees with the "as designed" matrix (Figure 3). Clearly, experimenters working on atmospheric structure experiments need to be aware of all aspects of their experiment and how uncertainties in even the least significant aspect can affect the accuracy of the final results. Requirements need to be defined, justified, and satisfied for every item that can affect the performance of the experiment and its results. This is perhaps most challenging for atmospheric structure experiments that are initially conceived as serving limited engineering purposes and only transform into scientific investigations at a late stage of their life cycle.

3. REDUCING NOISE

All atmospheric structure experiments work at their noise limits at high altitudes. Finding ways to reduce noise, thereby increasing vertical range upwards, is a common challenge. Averaging is the obvious approach to pursue, but at the cost of reducing vertical resolution. Yet the simple arithmetic mean is not appropriate here. The magnitude of a, the axial acceleration, increases exponentially with time at high altitudes (Figure 1). Thus:

$$a = a_0 \exp \frac{t}{\tau} \tag{1}$$

where t is time, a_0 is the acceleration at time $t = 0$, and τ is the timescale, which equals the ratio of the atmosphere's density scale height to the rate of change of altitude.

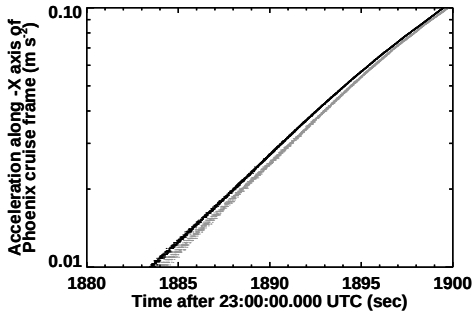

Figure 4. Two time series of axial acceleration measurements before bias correction. Grey dots indicate smoothing with a 1024 point (5.12 sec) running mean and black dots indicate smoothing with a 2048 point (10.24 sec) running mean.

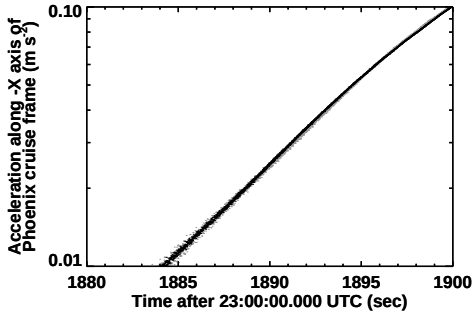

Figure 5. Two time series of axial acceleration measurements after bias correction. Grey dots indicate smoothing with a 1024 point (5.12 sec) running mean followed by correction using ratio to a 2048 point (10.24 sec) running mean. Black dots indicate smoothing with a 2048 (10.24 sec) point running mean followed by correction using ratio to a 4096 (20.48 sec) point running mean.

The mean acceleration between $t = -t_X$ and $t = t_X$, a_{mean}, is not the same as the desired acceleration at the centre of the time series unless $t_X \ll \tau$ (Withers et al. 2010):

$$a_{mean} = a_0 \frac{\tau}{t_X} \sinh\left(\frac{t_X}{\tau}\right) \tag{2}$$

Not only is the arithmetic mean a biased estimate of the desired quantity, but transition from one smoothing window to a different smoothing window (as might be applied to retain a constant fractional error whilst maximizing vertical resolution, for example) involves an unphysical discontinuous change in mean acceleration that is extremely problematic to deal with. However, if the timescale τ can be determined, then the value of a_0 can be found from a_{mean} and t_X. If a "long" average, a_L, and a "short" average, a_S, are calculated over the ranges

$t = -2t_S$ to $t = 2t_S$ and $t = -t_S$ to $t = t_S$, respectively, then the ratio of the averages satisfies:

$$\frac{a_L}{a_S} = \cosh\left(\frac{t_S}{\tau}\right) \tag{3}$$

Equation 3 can be rearranged using the trigonometric identity $\cosh^{-1}(x) = \ln\left(x + \left(x^2 - 1\right)^{1/2}\right)$ to yield:

$$\frac{t_S}{\tau} = \ln\left(\frac{a_L}{a_S} + \sqrt{\left(\frac{a_L}{a_S}\right)^2 - 1}\right) \tag{4}$$

Thus the timescale τ can be determined from the two related means, a_L and a_S, and then used to find the true acceleration at the centre of the series of data points. Figure 4 illustrates differences between a_L and a_S for the Phoenix data. Figure 5 shows how these differences are drastically reduced after application of the correction procedure outlined above.

4. ANGLE OF ATTACK INCONSISTENCIES

Since Phoenix carried gyroscopes, its angle of attack can be reconstructed directly, α_D, as shown in Figure 3. An independent indirect estimate of the angle of attack, α_I, can also be obtained from the ratio of normal to axial acceleration (Withers et al. 2010). The indirect α_I is often used to support the trajectory and atmospheric structure reconstruction for missions that carry accelerometers, but not gyroscopes (Spencer et al. 1999; Withers et al. 2003). Yet Figure 6 shows that α_I is typically 1–2 degrees smaller than α_D. Note that this issue is different from discrepancies between **predicted** and **reconstructed** angles of attack addressed by Desai et al. (2008). Resolution of this issue is important for understanding the flight dynamics of Phoenix and similar entry vehicles. Its precise implications are unclear, but they could be significant.

5. ANOTHER ROUTE TO ATMOSPHERIC DENSITY

Figures 3 and 6 show small oscillations in the angle of attack. They have amplitudes on the order of tenths of a degree and periods of about two seconds. The period of these oscillations depends on the atmospheric density (Schoenenberger et al. 2005):

$$\Omega^2 = \frac{-\rho V^2 A D C_{m\alpha}}{2I} \tag{5}$$

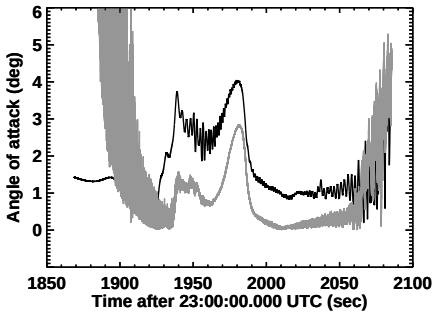

Figure 6. Time series of directly determined angle of attack, α_D, (black line) and indirectly determined angle of attack, α_I (grey line). Results after parachute deployment are not shown.

where Ω is the angular frequency of the oscillations, ρ is atmospheric density, V is atmosphere-relative speed, A is a reference area, D is a reference diameter, $C_{m\alpha}$ is the derivative of the pitching moment coefficient with respect to angle of attack, and I is a moment of inertia. If the observed period of oscillations, reconstructed density and speed, reference area of $\pi D^2/4$ where $D = 2.65$ m (Catling et al. 2008), and $C_{m\alpha} \sim 0.1$ rad s^{-1} (Edquist et al. 2008) are used with Equation 5 to calculate I, then the resultant I is within $\sim 10\%$ of 200 kg m^2 over much of the trajectory (Withers et al. 2010). The actual moment of inertia is close to 200 kg m^2 (Prince et al. 2008).

This technique can be inverted to obtain density estimates from the period of these oscillations, moment of inertia, and pitching moment coefficient. Its accuracy is likely to be worse than the standard "density from drag deceleration" method due to the potentially complex dynamics of real, not idealized, entry vehicles and uncertainties in the derivative of the pitching moment coefficient. Nonetheless, the accuracy of the technique should be estimated by a detailed study. Even if the formal uncertainties are relatively large, the technique may still be valuable as an independent verification of the results of the standard "density from drag deceleration" method.

6. YET ANOTHER ROUTE TO ATMOSPHERIC DENSITY

Many entry vehicles, including Phoenix, maintain a direct-to-Earth radio link during EDL or a similar radio link to a receiver capable of recording the received frequency. These data serve as an important source of information for understanding events during EDL, particularly in the event of mission failure during or shortly after EDL.

The time series of received frequencies could be used to perform a trajectory and atmospheric structure reconstruction independent of any accelerometer data recorded onboard the spacecraft during EDL. Near-real-time tra-

jectory and atmospheric structure reconstruction offers a number of benefits. First, it provides a rapid estimate of landing site location. Second, it provides a rapid assessment of the accuracy of the predicted atmospheric conditions. Third, it provides a set of immediate and tangible data products for the public to engage with. Public interest in the EDL phase of missions is intense, yet few results are available for discussion until a day or so later. Results would be available even if the spacecraft exploded upon ground impact without returning any science data.

The Doppler effect can be used to determine $\underline{v} \cdot \underline{l_0}$ from the received frequency at a given time, where $\underline{v}$ is the velocity of the spacecraft with respect to the known trajectory of the receiver and $\underline{l_0}$ is the unit vector along the line of sight from the spacecraft to the receiver. The velocity vector at time $t_1 = t_0 + dt$, $\underline{v_1}$, is related to the velocity vector at time t_0, $\underline{v_0}$, via the acceleration vector, $\underline{a}$:

$$\underline{v_1} = \underline{v_0} + \underline{a}\, dt \tag{6}$$

The acceleration vector, $\underline{a}$, is the sum of the gravitational acceleration, $\underline{g}$, and the aerodynamic acceleration, $\underline{a_{aero}}$:

$$\underline{a} = \underline{a_{aero}} + \underline{g} \tag{7}$$

Rearranging leads to:

$$\underline{a_{aero}} \cdot \underline{l_0} = \frac{1}{dt}\left(\underline{v_1} \cdot \underline{l_0} - \underline{v_0} \cdot \underline{l_0}\right) - \underline{g} \cdot \underline{l_0} \tag{8}$$

Under certain circumstances, it is reasonable to assume that $\underline{a_{aero}} = -k\left(\underline{v_0} - \underline{v_{\mathrm{atm}}}\right)$, where $\underline{v_{\mathrm{atm}}}$ is the velocity of the rotating planetary atmosphere (Withers et al. 2003). This is equivalent to the absence of lift on the entry vehicle. Thus:

$$\underline{a_{aero}} = \frac{\left(\underline{v_0} - \underline{v_{\mathrm{atm}}}\right)}{\left(\underline{v_0} \cdot \underline{l_0} - \underline{v_{\mathrm{atm}}} \cdot \underline{l_0}\right)} \times \left[\frac{1}{dt}\left(\underline{v_1} \cdot \underline{l_0} - \underline{v_0} \cdot \underline{l_0}\right) - \underline{g} \cdot \underline{l_0}\right] \tag{9}$$

All of the quantities on the right-hand side of Equation 9 are known, so $\underline{a_{aero}}$ can be inferred. The trajectory and atmospheric structure reconstruction can proceed as usual without needing any onboard accelerometer data. This concept has been applied to received frequencies recorded during the EDL of Opportunity, which are shown in Figure 7. Note that the labels on the horizontal axis of Figure 7 are incorrect. Results are shown

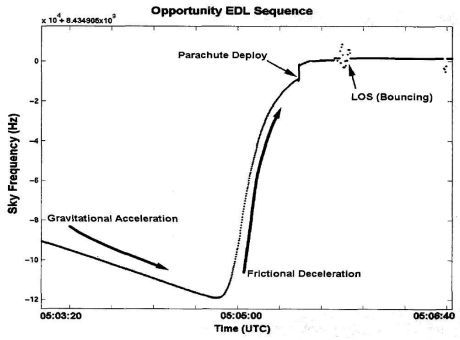

Figure 7. Sky frequency observed by the NASA Deep Space Network during the EDL of Opportunity. The effects of atmospheric drag (frictional deceleration) are clearly visible. From Johnston et al. (2004).

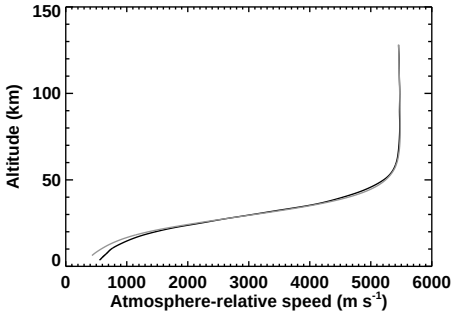

Figure 8. Atmosphere-relative speed determined from Opportunity's direct-to-Earth transmissions (black line) and from the accelerometer-based reconstruction of Withers & Murphy (2009) (grey line) as functions of altitude.

in Figures 8 and 9. Given the inaccuracies introduced by extracting time and frequency data from Figure 7, the results are promising. It is clear that significantly greater accuracy would be obtained if the actual time series of received frequencies was used instead. Two steps are necessary before this technique can be relied upon to support future entry probes formally. First, it should be demonstrated using actual received frequencies, not values extracted from a published figure. Possible test cases include the Pioneer Venus probes (Counselman et al. 1980), Pathfinder (Wood et al. 1997), Spirit, Opportunity, Phoenix (Kornfeld et al. 2008), the Galileo probe (Atkinson et al. 1998), and Huygens (Bird et al. 2005; Folkner et al. 2006). Second, sensitivity studies and error analyses should be performed to quantify the expected accuracy of its results.

7. SCIENCE

Figure 10 shows the reconstructed temperature profile for Phoenix (Withers & Catling 2010). The mesopause is clearly detected near 100 km, but temperature uncertain-

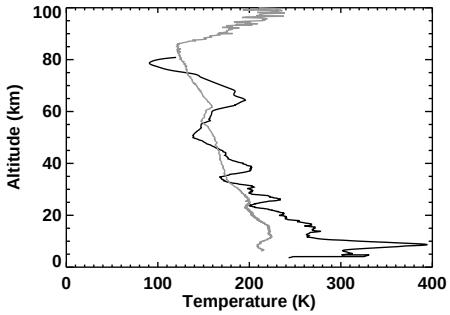

Figure 9. Temperature determined from Opportunity's direct-to-Earth transmissions (black line) and from the accelerometer-based reconstruction of Withers & Murphy (2009) (grey line) as functions of altitude.

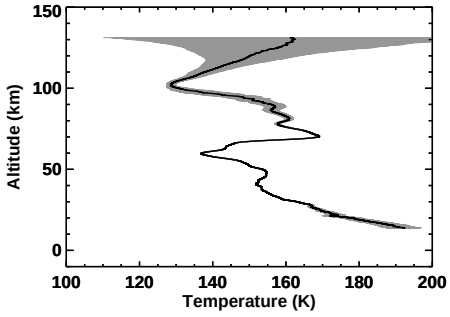

Figure 10. Vertical profile of reconstructed temperature for Phoenix (black solid line), with 1σ temperature uncertainties shown by the grey envelope.

ties become very large at higher altitudes in the thermosphere. The middle atmosphere is dominated between 60 km and 100 km by a large temperature maximum that is 30 K warmer than its flanking temperature minima. This is caused by the sun-synchronous diurnal thermal tide, which a major component of the dynamics of the atmosphere of Mars. Below 60 km, temperatures increase more-or-less monotonically with decreasing altitude. The small temperature maximum at 48 km may also be associated with the sun-synchronous diurnal thermal tide.

Figure 11 shows all six entry profiles obtained from the martian atmosphere to date. The overall impression is that temperatures increase steadily with increasing pressure for pressures greater than 1 Pa, but vary significantly for smaller pressures.

These profiles are challenging to interpret due to their small number. Orbital measurements offer much larger numbers of atmospheric profiles at a range of latitudes, local times, and seasons. These permit studies of the three-dimensional structure of the martian atmosphere that the limited entry profiles do not. However, entry profiles offer unique vertical range and resolution. Indeed, their vertical resolution is much better than typical global-scale general circulation models, and hence many

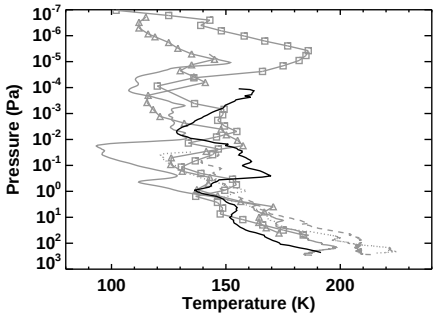

Figure 11. Six temperature-pressure profiles obtained by Mars landers. Viking 1 is shown by the grey solid line marked with squares, Viking 2 by the grey solid line marked with triangles, Pathfinder by the unmarked grey solid line, Spirit by the grey dashed line, Opportunity by the grey dotted line, and Phoenix by the black solid line.

of the interesting phenomena contained in the entry profiles are produced by "sub-grid-scale processes" that are represented parametrically in such models. The historical division of many aspects of the atmospheric sciences into "lower atmosphere," "middle atmosphere," or "upper atmosphere" topics has meant that many studies have not taken full advantage of the ability of entry profiles to sample all these vertical regions at the same location and time. Increasing recognition of the importance of coupling between atmospheric regions — and the resultant stimulus to develop "whole atmosphere" general circulation models with vertical ranges comparable to those of entry profiles — means that future analyses of entry profiles may make greater use of their full vertical extent. One-dimensional models are more able to match the vertical range and resolution of entry profiles, but cannot fully include the atmospheric dynamics that influence so many aspects of the observed thermal structure.

8. SUMMARY

Phoenix landed safely on the surface of Mars as designed. Measurements made during its entry have been used to reconstruct its trajectory and the atmospheric density, pressure, and temperature along this trajectory. Challenges faced during the reconstruction process included uncertainties in the relationship of key reference frames and noisy data. The results of the trajectory reconstruction are self-consistent and consistent with other constraints. Two different methods for determining the angle of attack during entry delivered significantly different results, the implications of which are not yet clear. Two alternative methods for finding atmospheric density have been discussed as possible complements to the established and robust "density from drag" method. The reconstructed temperature profile shows strong influences of the sun-synchronous diurnal thermal tide in the middle atmosphere. This is the sixth entry profile from the atmosphere of Mars and the first from the polar regions,

which play an important role in determining the climate of Mars.

ACKNOWLEDGMENTS

PW acknowledges support from NASA (NNX09AG16G). DC acknowledges past support from the UK Science and Technology Facilities Council (STFC) awarded to the University of Bristol for Phoenix lander data reduction. PW and DC also acknowledge help and assistance from many people associated with the Phoenix project.

REFERENCES

Arvidson, R. E., Bonitz, R. G., Robinson, M. L., et al. 2009, J. Geophys. Res., 114, E00E02, 10.1029/2009JE003408

Atkinson, D. H., Pollack, J. B., & Seiff, A. 1998, J. Geophys. Res., 103, 22911

Bird, M. K., Allison, M., Asmar, S. W., et al. 2005, Nature, 438, 800

Blanchard, R. C. 2009, in Report produced by George Washington University under NASA grant award CCLS20458F and subsequently submitted to Journal of Spacecraft and Rockets

Catling, D. C., Beebe, R. F., Murphy, J. R., & Huber, L. F. 2008, in PHX-M-ASE-2-EDL-V1.0, NASA Planetary Data System

Counselman, C. C., Gourevitch, S. A., King, R. W., Loriot, G. B., & Ginsberg, E. S. 1980, J. Geophys. Res., 85, 8026

Desai, P. N., Prince, J. L., Queen, E. M., Cruz, J. R., & Grover, M. R. 2008, in American Institute of Aeronautics and Astronautics paper 2008-7346, AIAA/AAS Astrodynamics Specialist Conference and Exhibit in Honolulu, Hawaii, USA

Edquist, K. T., Desai, P. N., & Schoenenberger, M. 2008, in American Institute of Aeronautics and Astronautics paper 2008-7219, AIAA/AAS Astrodynamics Specialist Conference and Exhibit in Honolulu, Hawaii, USA

Folkner, W. M., Asmar, S. W., Border, J. S., et al. 2006, J. Geophys. Res., 111, E07S02, 10.1029/2005JE002649

Grover, M. R., Cichy, B., & Desai, P. N. 2008, in American Institute of Aeronautics and Astronautics paper 2008-7218, AIAA/AAS Astrodynamics Specialist Conference and Exhibit in Honolulu, Hawaii, USA

Guinn, J. R., Garcia, M. D., & Talley, K. 2008, J. Geophys. Res., 113, E00A26, 10.1029/2007JE003038

Johnston, D., Asmar, S., Chang, C., et al. 2004, in 3rd International Workshop on Tracking Commands Systems, Darmstadt, Germany, 7-10 September 2004, http://hdl.handle.net/2014/39097

Kornfeld, R. P., Garcia, M. D., Craig, L. E., Butman, S., & Signori, G. M. 2008, J. Spacecraft and Rockets, 45, 534

Prince, J. L., Desai, P. N., Queen, E. M., & Grover, M. R. 2008, in American Institute of Aeronautics and Astronautics paper 2008-7507, AIAA/AAS Astrodynamics Specialist Conference and Exhibit in Honolulu, Hawaii, USA

Schoenenberger, M., Hathaway, W., Yates, L., & Desai, P. N. 2005, in American Institute of Aeronautics and Astronautics paper 2005-0055, 43rd AIAA Aerospace Science Meeting in Reno, Nevada, USA

Smith, D., Neumann, G., Arvidson, R. E., Guinness, E. A., & Slavney, S. 2003, in MGS-M-MOLA-5-MEGDR-L3-V1.0, NASA Planetary Data System

Smith, P. H., Tamppari, L., Arvidson, R. E., et al. 2008, J. Geophys. Res., 113, E00A18, 10.1029/2008JE003083

Smith, P. H., Tamppari, L. K., Arvidson, R. E., et al. 2009, Science, 325, 58

Spencer, D. A., Blanchard, R. C., Braun, R. D., & W., T. S. 1999, J. Spacecraft and Rockets, 36, 357

Withers, P. & Catling, D. C. 2010, Geophys. Res. Lett., under review

Withers, P., Catling, D. C., & Murphy, J. R. 2010, in PHX-M-ASE-5-EDL-RDR-V1.0, NASA Planetary Data System

Withers, P. & Murphy, J. R. 2009, in MER1/MER2-M-IMU-5-EDL-DERIVED-V1.0, NASA Planetary Data System

Withers, P., Towner, M. C., Hathi, B., & Zarnecki, J. C. 2003, Planet. Space Sci., 51, 541

Wood, G. E., Asmar, S. W., Rebold, T. A., & Lee, R. A. 1997, JPL TDA Progress Report 42-131, available online at http://ipnpr.jpl.nasa.gov/progress_report/42-131/131I.pdf